Evaluation of Quantitative Criteria for Glioma Grading With Static and Dynamic ^{18}F-FDopa PET/CT

Christophe Nioche, PhD, Marine Soret, PhD,* Eric Gontier, MD,* Marion Lahutte, MD,* Guillaume Dutertre, MD,* Renaud Dulou, MD,* Laurent Capelle, MD,† Rémy Guillevin, MD, PhD,† Hervé Foehrenbach, MD,* and Irène Buvat, PhD‡*

Purpose: The aim of this study was to compare various acquisition and processing protocols for noninvasive glioma grading using either static or dynamic ^{18}F-FDopa PET.

Methods: Dynamic studies were performed in 33 patients. Based on histopathological analysis, 18 patients had a high-grade (HG) tumor and 15 patients had a low-grade (LG) tumor. For static imaging, SUV_{mean} and SUV_{max} were calculated for different acquisition time ranges after injection. For dynamic imaging, the transport rate constant k_1 was calculated according to a compartmental kinetic analysis using an image-derived input function.

Results: With the use of a 5-minute static imaging protocol starting at 38 minutes after injection, newly diagnosed HG tumors could be distinguished from LG tumors with a sensitivity of 70% and a specificity of 90% with a threshold of SUV_{mean} of 2.5. In recurrent tumors, a sensitivity of 100% and a specificity of 80% for identifying HG tumors were obtained with a threshold set to 1.8. Dynamic imaging only slightly, but nonsignificantly, improved differential diagnosis.

Conclusions: Static and dynamic imaging without blood sampling can discriminate between LG and HG for both newly diagnosed and recurrent gliomas. In dynamic imaging, excellent discrimination was obtained by considering the transport rate constant k_1 of tumors. In static imaging, the best discrimination based on SUV was obtained for SUV_{mean} calculated from a 5-minute acquisition started at 38 minutes after injection.

Key Words: brain imaging, dopamine, kinetic modeling, neurooncology, PET

(*Clin Nucl Med* 2013;38: 81–87)

Brain imaging is a promising approach for noninvasive tumor grading.[1] The potential of PET/CT imaging for grading brain tumors PET/CT with labeled amino acids or analogs, such as methionine, tyrosine, leucine, alanine, and isobutyric acid, has been reported, involving either dynamic[2] or static studies.[3,4] The clinical application of dynamic analysis of L-3,4-dihydroxy-6-^{18}F-fluoro-phenyl-alanine (^{18}F-FDopa) in brain tumors has also been described.[2,5,6] Chen et al[7] found no significant difference between high-grade (HG) and low-grade (LG) brain tumors using the SUV_{max} in the tumor for static ^{18}F-FDopa ($P = 0.40$) with 7 newly diagnosed and 23 recurrent tumors, where the static images were obtained using 20-minute acquisition starting 10 minutes after injection. Schiepers et al[8] reported significant differences ($P < 0.01$) between HG and LG brain tumors using dynamic ^{18}F-FDopa and static ^{18}F-FDopa with 16 newly diagnosed and 35 recurrent tumors, without determining whether dynamic imaging should be preferred. Using static PET imaging (20-minutes acquisition starting at 10 minutes after injection) and SUV, Fueger et al[9] also found a significant difference ($P = 0.001$) between HG and LG brain tumors for 22 newly diagnosed tumors but not for 37 recurrent tumors ($P = 0.41$). They suggested that ^{18}F-FDopa could be useful for distinguishing tumor recurrence from radiation necrosis. So far, there are not much published data regarding the comparison between the diagnostic performance of static and dynamic ^{18}F-FDopa PET imaging.[6]

In this work, we investigated several acquisition and processing protocols of noninvasive ^{18}F-FDopa PET/CT (without blood sampling) for glioma grading. We compared the accuracy of tumor grading based on tumor SUV_{mean} and SUV_{max} calculated using static PET/CT corresponding to various time ranges after acquisition and based on the influx rate constants measured using a dynamic acquisition and an image-derived arterial input function. Static and dynamic methods have never been compared in this context. A goal was to determine if a static acquisition could distinguish HG and LG brain gliomas or if dynamic imaging with compartmental analysis was needed.

PATIENTS AND METHODS

Patients

Thirty-three patients (5 women, 28 men) were scanned using PET/CT (Table 1) without carbidopa premedication and fasting. The mean (SD) patient age was 51 (16) years (range, 22–97 years). Ten patients presented with recurrent tumors and previously received antiepileptic treatment (levetiracetam or sodium valproate). All 10 went through surgical resection. In addition to surgery, 7 patients received chemotherapy (temozolomide [alkylating agent] or bevacizumab, and irinotecan [antiangiogenaic therapy]) or radiation, whereas 1 patient underwent radiation therapy only. Three patients presented with recurrent tumors and had not received treatment. Twenty patients presented with newly diagnosed tumors and had received antiepileptic treatment without chemotherapy and radiation. The protocol was approved by our ethics committee, and informed consent was given by patients or their relatives.

PET/CT IMAGING

The recommended injected activity was 2.2 MBq/kg per patient. Patients were injected with activities between 120 and 200 MBq of ^{18}F-FDopa (IASOdopa, IASON GmbH, Graz, Austria). Images were acquired with a PET/CT GEMINI TF (Philips Healthcare, Cleveland, OH).

First, a thoracic CT acquisition was performed (120 kV, 100 mA, pitch:1:1, 60-cm transverse FOV, 512 × 512 pixels, 2 × 2-mm^2 pixel size, and 2-mm thickness). Then, a dynamic thorax PET acquisition of 1-minute 50-second duration was started at the time of tracer injection (between 5 and 7 mL per 30 seconds). One bed position (18-cm longitudinal FOV) including the thorax and centered on the heart was acquired in list mode. This 1-minute 50-second dynamic acquisition was reconstructed in 10 frames of 11 seconds

Received for publication June 2, 2012; revision accepted September 27, 2012.

From the *Hôpital d'Instruction des Armées du Val-de-Grâce 74, bd du Port Royal; †UMR 678 INSERM AP-HP Groupe Hospitalier Pitié-Salpêtrière, Paris; and ‡UMR 8165 CNRS Imagerie et Modélisation en Neurobiologie et Cancérologie Orsay, France.

Conflicts of interest and sources of funding: none declared.

Reprints: Christophe Nioche, PhD, (Fédération d'Imagerie Médicale), Hôpital d'Instruction des Armées du Val-de-Grâce 74, bd du Port Royal, 75005 Paris, France. E-mail: christophe.nioche@gmail.com.

ISSN: 0363-9762/13/3802–0081

TABLE 1. Patient Characteristics

Characteristics	All Patients (n = 33)	Newly Diagnosed (n = 20)	Recurrent (n = 13)
Age, n			
Median, y	51	50	53
Range, y	22–97	22–97	35–72
Duration disease, n			
Median, wk	169	49	354
Range, wk	2–708	2–193	88–708
Sex, n (%)			
Female	5 (15)	3 (15)	2 (15.4)
Male	28 (85)	17 (85)	11 (84.6)
Tumor volumes, cm^3			
LG, mean (SD), range	13.4 (10.4), 0.5–31.4	14.7 (11.3), 0.5–31.4	7.9 (2.5), 7.5–15.2
HG, mean (SD), range	35.7 (36.1), 3.9–123.4	28.5 (36.3), 3.9–114.0	34.0 (38.3), 5.7–123.4
Histopathology, n (%)			
LG	**15 (46)**	**10 (50)**	**5 (38.5)**
WHO grade I	0 (0)	0 (0)	0 (0.0)
WHO grade II	15 (46)	10 (50)	5 (38.5)
Gemistocytic-astrocytoma	2 (6)	2 (10)	0 (0.0)
Oligodendroglioma	11 (34)	7 (35)	4 (30.8)
Oligoastrocytoma	2 (6)	1 (5)	1 (7.7)
HG	**18 (54)**	**10 (50)**	**8 (61.5)**
WHO grade III	10 (30)	5 (25)	5 (38.5)
Oligodendroglioma	7 (21)	4 (20)	3 (23.1)
Anaplastic-oligoastrocytoma	2 (6)	1 (5)	1 (7.7)
Astrocytoma	1 (3)	0 (0)	1 (7.7)
WHO grade IV	8 (24)	5 (25)	3 (23.1)
Glioblastoma	7 (21)	5 (25)	2 (15.4)
Oligodendroglioma	1 (3)	0 (0)	1 (7.7)

using the 3D OSEM algorithm including attenuation and scatter corrections. The reconstructed voxel size was $4 \times 4 \times 4\text{-mm}^3$ (smallest voxel size achievable in our scanner for a thorax acquisition). The motivation for this initial thoracic acquisition was to obtain an accurate image-derived arterial input function (IDAIF) of ^{18}F-FDopa. For each thorax PET/CT, a 10-mm thick volume of interest (VOI) in the descending aorta was drawn manually on the CT images and used to estimate the IDAIF.[10] The PET activity measurements in the aorta VOI were corrected from partial volume effect using a recovery coefficient method.[11] The recovery coefficient was calculated by convolving the binary aorta VOI with a 3D Gaussian function (6.5-mm full width at half maximum), modeling the point spread function in the reconstructed images. The 6.5-mm value was measured using a glass capillary filled with ^{18}F, after acquiring and reconstructing the data using exactly the same protocol as in patients. Only spill-out activity was compensated for. Activity from outside the aorta detected within the aorta VOI could be neglected, thanks to very early acquisition, before significant tissue distribution of the tracer and the lack of any radioactivity accumulation close to the aorta at this time.

For each patient, we visually checked the aorta ^{18}F-FDopa time-activity curve (TAC) (blue line in Fig. 1A and B). As the IDAIF was not sampled after 1 minute 50 seconds, we completed the curve up to 40 minutes as needed by the subsequent compartmental analysis, by fitting the decreasing part of the aorta curve with a decreasing monoexponential function: $y = a \exp(-t / b) + c$ (red line in Fig. 1A and B). The c offset value accounted for the residual ^{18}F-FDopa in the blood. Its value was estimated as the averaged c value obtained using exactly the same model on a set of 20 AIF measured in ^{18}F-FDopa scans acquired as part of a different research protocol, including a late image on the aorta. The green points in Figure 1A correspond to the c values obtained in these 20 patients, at the times at which the late scan was acquired. The values resulting from the fit were used to complete the decreasing part of the aorta up to 40 minutes, with a time sampling of 30 seconds.

A dynamic brain PET acquisition of 40 minutes duration was performed after the thoracic acquisition. One bed position (transaxial FOV, 25.6 cm) centered on the brain was acquired in list mode, starting 3 minutes after the injection of ^{18}F-FDopa. The reconstructed voxel size was $2 \times 2 \times 2\text{-mm}^3$. For the static image analysis, a PET image corresponding to the 40-minute acquisition was reconstructed. In addition, 2 time frames were reconstructed based on the method in Schiepers et al[8]: one corresponding to 15 to 25 minutes and a late interval corresponding to the last 5 minutes of our dynamic acquisition (38–43 minutes after injection). The 40-minute dynamic acquisition was also reconstructed in 40 frames of 1 minute for kinetic modeling. Owing to the dynamic imaging protocol, no imaging was performed after 43 minutes, to avoid keeping the patients longer on the scanning table.

The approximately 1-minute time lag between the thoracic and brain acquisitions was necessary for shifting the bed, repositioning the patient's arms along the body, and triggering the camera for the brain acquisition.

The brain CT acquisition was performed after the PET acquisition (120 kV, 150 mA, pitch:1:1, 60-cm transverse FOV, 512×512 pixels, $2 \times 2\text{-mm}^2$ pixel size, and 2-mm thickness) without iodine IV contrast agent. Reconstructed images were 2-mm thick and had $2 \times 2\text{-mm}^2$ pixel size. For thorax and brain, the CT volume was used for

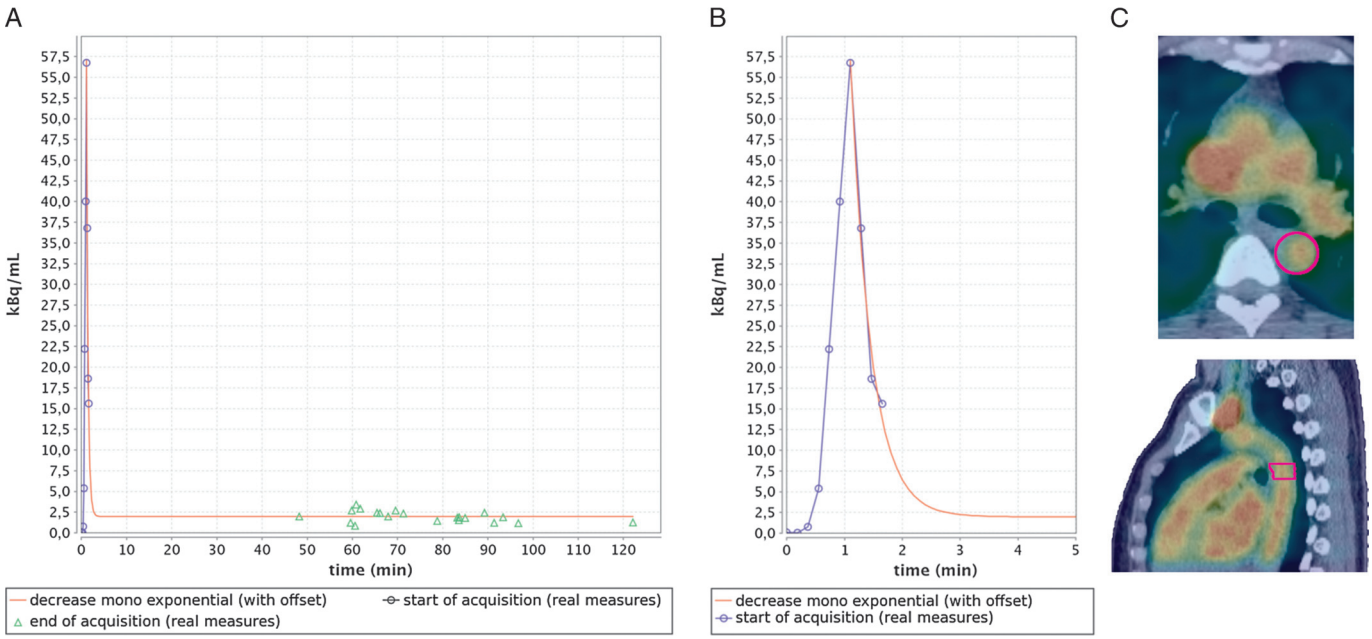

FIGURE 1. **A**, time-activity curve (blue) derived from the aorta VOI with partial volume correction with the result of the monoexponential fit of the decreasing part of the curve (red). A set of 20 points obtained from late ^{18}F-FDopa acquisitions performed in other patients are shown in green. These points were used to determine the averaged offset of the IDAIF (discussed in the text). **B**, Same as **A** with 5-minute range. **C**, Fused CT and ^{18}F-FDopa PET slices, with the aorta VOI shown in magenta.

attenuation correction and as an anatomic reference for PET/CT image fusion.

Image Analysis

Images were first inspected visually, then static and dynamic data were analyzed. For each subject, a 2-dimensional circular tumor region of interest (ROI) with a volume of 35-mm^3 was automatically drawn and centered on the voxel with the SUV_{max} in the PET static image of 40-minute duration. This same ROI was applied to both static and dynamic analyses. Another VOI was manually drawn on the PET static image of 40-minute duration to determine the tumor volume, by encompassing all the tumor areas. All HG and LG tumors were relatively easy to delineate, thanks to the high contrast between tumor and background. The number of voxels in this VOI was converted into a tumor volume.

Static Image Analysis

The tumor SUV_{mean} and SUV_{max} were calculated within the tumor ROI for the 3 acquisition times. The first time range (between 15 and 25 minutes after injection, called *median*) yielded $SUV_{mean,median}$ and $SUV_{max,median}$. The second interval (between 38 and 43 minutes after injection, called *late*) yielded $SUV_{mean,late}$ and $SUV_{max,late}$. The third interval (between 3 and 43 minutes after injection, called *total*) yielded $SUV_{mean,total}$ and $SUV_{max,late}$.

Nonparametric receiver operating characteristic (ROC) curve analysis was used for all time ranges to characterize the performance of all SUV indices in distinguishing between HG and LG tumor (ROCR[12]).

Dynamic Image Analysis

We used a 2-compartment model adapted from the one used by Schiepers et al,[8] without metabolite correction. The first compartment was the arterial blood mean activity [C_p]. From arterial blood, the radiotracer passes into the so-called free compartment (f) corresponding to nonspecific (n) uptake and specific uptake (b) or metabolism mean activity [C_{fnb}]. The transport and uptake rates of the tracer k_1 (in mL/g/min) for transport of [C_p] to [C_{fnb}], k_2 (per minute) for transport of [C_{fnb}] to [C_p] are assumed to be linearly related to the concentration differences between the 2 compartments C_p and C_{fnb}. If $C_p(t)$ and $C_{fnb}(t)$ are the radioactivity concentrations at time t, in minutes, for each compartment, the measured PET data corresponds to $C_{PET}(t) = C_p(t) + C_{fnb}(t)$.

The model parameters can be estimated by fitting the model to the measured PET data, using the arterial radioactivity concentration $C_p(t)$ as the input function. For our clinical study, including only outpatients, the arterial input function was estimated as described in PET/CT Imaging section.

Our kinetic model was solved using Lawson-Hanson nonnegative least square algorithm,[13] from the Turku PET Center library open source software (c/o Turku University Hospital, Kiinamyllynkatu 4–8, 20520 Turku, Finland).

Receiver operating characteristic curve analysis was used to assess the performance of the transfer rate k_1 in discriminating between LG and HG tumors (ROCR[12]).

Statistical Analysis

The significance of the difference between the areas under the ROC curves was tested using a nonparametric test, with $P < 0.05$ considered as significant.[14]

RESULTS

Histopathology

The distribution of tumor types, grades, and volumes is listed in Table 1. Of the patients, 18 (54%) had an HG tumor and 15 (46%) had an LG tumor. Seven tumors (21%) were classified as glioblastoma, 19 (57.6%) as oligodendroglioma. Of 28 lesions, 8 (24%) were classified as grade IV, 10 (30%) as grade III, and 15 (46%) as grade

TABLE 2. Static Imaging Analysis

	All Tumors			Newly Diagnosed Tumors			Recurrent Tumors		
	HG*	LG*	P†	HG*	LG*	P†	HG*	LG*	P†
$SUV_{mean,median}$	3.6 (1.0)	2.1 (0.2)	0.001	3.4 (0.8)	2.3 (1.0)	0.015	3.8 (1.2)	1.8 (0.8)	0.009
$SUV_{mean,late}$	2.7 (0.8)	1.6 (0.6)	0.001	2.6 (0.6)	1.7 (0.6)	0.006	3.0 (1.0)	1.5 (0.5)	0.010
$SUV_{mean,total}$	3.5 (1.0)	2.0 (0.9)	0.001	3.2 (0.8)	2.1 (1.0)	0.012	3.8 (1.3)	1.8 (0.8)	0.009
$SUV_{max,median}$	4.4 (1.2)	2.9 (1.3)	0.002	4.2 (0.9)	3.1 (1.3)	0.042	4.7 (1.6)	2.8 (1.6)	0.067
$SUV_{max,late}$	3.1 (0.9)	2.1 (0.8)	0.001	3.0 (0.6)	2.1 (0.8)	0.019	3.3 (1.1)	2.3 (1.3)	0.147
$SUV_{max,total}$	4.3 (1.4)	2.6 (1.2)	0.001	4.0 (1.3)	2.5 (1.0)	0.008	4.6 (1.4)	2.8 (1.7)	0.066

*Data are presented in mean (SD) SUV.

†Bilateral *t* test (Student) of HG versus LG; $P < 0.05$ was considered significant.

II, and there was no grade I lesion. Twenty lesions were newly diagnosed, and 13 were recurrent brain tumors.

Only 1 LG tumor had a volume less than 2.9 cm^3, whereas all HG tumors were larger than 3.9 cm^3. Given the spatial resolution in our reconstructed images (6.5 mm), partial volume effect should thus not introduce a large bias in our measurements.

Static Imaging

When considering all tumors, whatever the time interval and for SUV_{mean} and SUV_{max}, there was a significant difference ($P < 0.02$) between the SUV measured in the HG and LG tumors (Table 2).

Figure 2 shows 2 PET static (40 minutes) slices and an example of typical TACs for HG (Fig. 2A) and LG (Fig. 2B) tumors. The cerebellum curves illustrate TACs measured in healthy tissue.

As expected from the TAC seen in Figure 2, for all tumors (HG and LG), on average, $SUV_{mean,median}$ had a higher value than $SUV_{mean,late}$ (Table 2).

When considering newly diagnosed and recurrent tumors together, the ROC curves describing the discrimination between HG and LG tumors are shown in Figure 3A for $SUV_{mean,late}$ (mean [SD] area under the curve [AUC], 0.88 [0.06]). The AUCs is given in Table 4, as well as the threshold (1.8) corresponding to the operating point (OP) maximizing the sum of sensitivity and specificity, and associated sensitivity and specificity (66% specificity and a 94% sensitivity). Similarly, the AUC, OP threshold, and corresponding sensitivity and specificity are given for all indices and all tumor groups in Table 4.

In the newly diagnosed tumors only, there was also a significant difference between HG and LG tumors whatever the SUV index ($P < 0.05$) (Table 2). Figure 3B shows the corresponding ROC curves, and Table 4 presents their characteristics.

In the recurrent tumors only, only the SUV_{mean} indices were significantly different between HG and LG tumors ($P < 0.01$), whereas the SUV_{max} indices were not ($P > 0.06$) (Table 2). Figure 3C shows the corresponding ROC curves, and Table 4 presents their characteristics.

The comparison of the AUC corresponding to the different SUV for a given group of tumors (all, newly diagnosed only, or recurrent only) did not show any statistically significant difference.

Dynamic Imaging

An example of aorta VOI in the axial (Fig. 1C, top) and sagittal (Fig. 1C, bottom) images is shown in Figure 1. The TAC in the VOI corresponds to the first 1.5 minutes of acquisition after injection (Fig. 1A and B, blue). It shows ^{18}F-FDopa passing through the aorta, yielding an estimate of the arterial input function. The result of the monoexponential fit of the decreasing part of the curve is also shown (Fig. 1A and B, red).

The highest tracer uptake in the HG tumors occurred at 8.5 (1.6) minutes and at 8.0 (2.9) minutes for LG tumors (no-significant [NS]).

Table 3 summarizes the k_1 and k_2 values for all tumors and for the subgroups of newly diagnosed and recurrent tumors. When considering all tumors, mean k_1 was significantly different between LG and HG ($P < 0.02$), unlike mean k_2. The same was true for newly diagnosed and recurrent tumors (Table 3).

The ROC curves for k_1 are shown in Figure 3A to C for the different tumor groups, and the corresponding curve features are summarized in Table 4.

There was no statistically significant difference between the AUC obtained with k_1 for the newly diagnosed tumors and the recurrent tumors, suggesting that FDopa PET kinetic analysis could

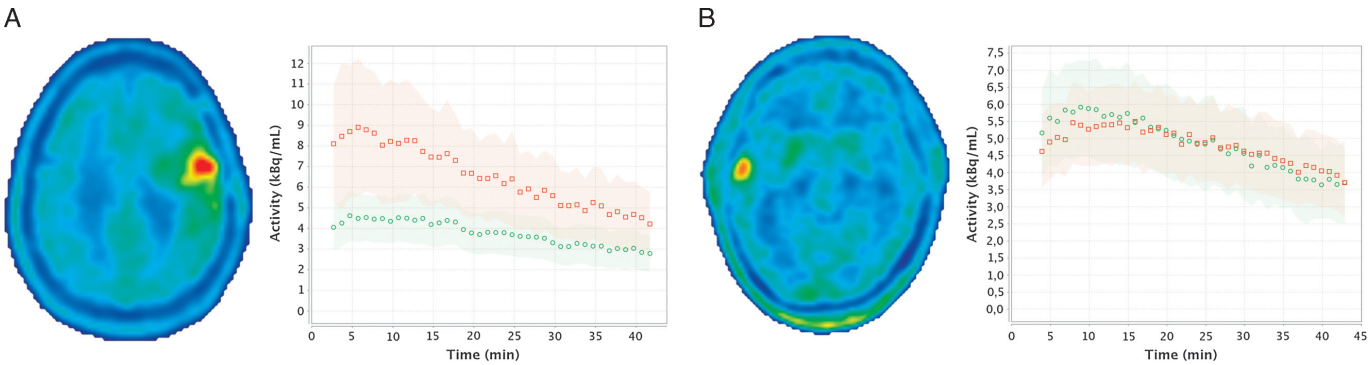

FIGURE 2. Forty-minute PET scan and corresponding ^{18}F-FDopa time-activity curves for the tumor (red) and cerebellum (green). The shaded colors represent 1 SD. **A**, HG tumor. **B**, LG tumor.

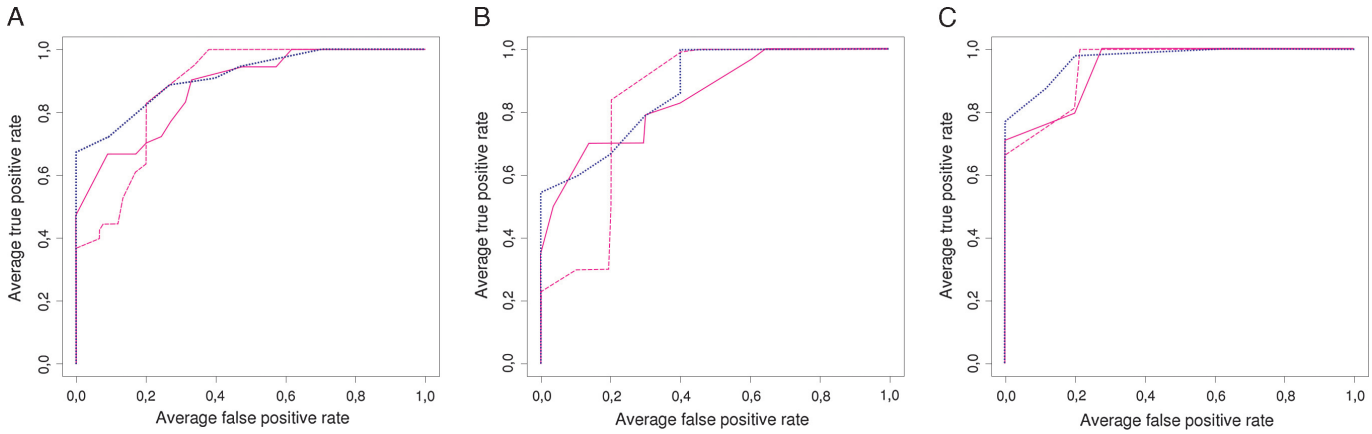

FIGURE 3. Receiver operating characteristic curves for k_1 (dotted blue curves), $SUV_{mean,late}$ (magenta plain curves), and $SUV_{mean,total}$ (magenta dotted curves) for all tumors (**A**), newly diagnosed tumors (**B**), and recurrent tumors (**C**).

distinguish between HG and LG tumors not only for newly diagnosed tumors but also for recurrent tumors.

DISCUSSION

We analyzed differences in ^{18}F-FDopa SUVs, k_1 and k_2 between HG and LG lesions in both newly diagnosed and recurrent gliomas. We also described a new noninvasive approach to estimate k_1 from dynamic imaging without any blood sampling.

Static Imaging for Grading Gliomas

Based on our dynamic acquisition protocol, we considered 3 static acquisition times after injection. Our group composed of all tumors demonstrate that HG tumors could be distinguished from LG tumors using all SUV_{mean} indices, whatever the postinjection acquisition time ($SUV_{mean,median}$, $SUV_{mean,late}$, and $SUV_{mean,total}$) with $P = 0.001$ (Table 2). Although the highest AUC at 0.88 (0.06) was observed for $SUV_{mean,late}$, our sample could not yield evidence of any statistically significant difference between AUC associated with $SUV_{mean,median}$, $SUV_{mean,late}$, and $SUV_{mean,total}$: all acquisition times yielded close results in terms of differential diagnosis.

In their study (11 newly diagnosed lesions, 28 recurrent tumors, and 27 clinically stable patients), Chen et al[7] found no significant difference between 18 LG and 48 HG tumors based on ^{18}F-FDopa uptake ($P = 0.40$) when using a static image of 10 to 30 minutes after injection and measuring the ratio of tumor to contralateral normal tissue uptake. No result regarding the discrimination of the HG and LG lesions based on SUV was included.

Focusing on newly diagnosed tumors only, our results demonstrate that HG tumors could be distinguished from LG tumors based on SUV_{mean} and on SUV_{max} with the median, late, and total time range ($P < 0.05$). The HG and LG recurrent tumors could be distinguished using static imaging only with SUV_{mean}. This might be due to the variability of SUV_{max}, which is more affected by noise than SUV_{mean} because SUV_{max} is calculated from a single voxel and/or to the lack of statistical power due to the relatively small number of patients in our subgroups. Our results therefore suggest that SUV_{mean} should be preferred for differential diagnosis between HG and LG tumors using static imaging and that when using SUV_{mean}, HG and LG gliomas could be identified for all acquisition times we considered and whatever the type of tumors (newly diagnosed or recurrent tumors).

The early acquisition time in the study by Schiepers et al[8] (15–25 minutes for 33 newly diagnosed lesions) corresponds to our median acquisition time. They found a trend toward higher uptake values for HG tumors, with a large overlap between tumor grades. This is consistent with our results as we found a significant difference between HG and LG newly diagnosed tumors for $SUV_{mean,median}$ ($P = 0.015$). In our clinical context, we could not confirm that optimal discrimination between HG and LG tumors in a static image was obtained 60 to 70 minutes after injection as reported by Schiepers et al.[8] The difference in grading accuracy observed at 38 minutes

TABLE 3. Dynamic Imaging Analysis 2C2p*

	k_1 (per min)	k_2 (per min)	WSS†
All tumors			
HG			
Mean (SD)	0.299 (0.144)	0.096 (0.057)	63 (51)
Range	0.124–0.570	0.003–0.251	15–224
LG			
Mean (SD)	0.125 (0.062)	0.077 (0.045)	53 (90)
Range	0.003–0.223	0.001–0.168	5–370
P‡	0.001	0.292	
Newly diagnosed tumors			
HG			
Mean (SD)	0.244 (0.098)	0.096 (0.065)	47 (27)
Range	0.124–0.464	0.024–0.251	15–92
LG			
Mean (SD)	0.121 (0.072)	0.071 (0.046)	35 (25)
Range	0.003–0.223	0.001–0.144	9–84
P‡	0.005	0.337	
Recurrent tumors			
HG			
Mean (SD)	0.369 (0.168)	0.097 (0.048)	83 (68)
Range	0.162–0.570	0.003–0.152	21–224
LG			
Mean (SD)	0.134 (0.039)	0.088 (0.046)	89 (158)
Range	0.086–0.192	0.056–0.168	5–370
P‡	0.012	0.768	

*Analyzed with 2 compartments and 2 parameters.

†Minimum weighted sum of squares (residual error using Lawson-Hanson nonnegative least square algorithm).

‡Bilateral t test (Student) of HG versus LG; $P < 0.05$ was considered significant.

TABLE 4. Results for Distinguishing Between LG and HG tumors Using Different Indices

Method	AUC ± SE	OP Threshold	Sensitivity, %	Specificity, %
All tumors				
Dynamic k_1	0.92 ± 0.05	0.226	72	100
Static $SUV_{mean,late}$	0.88 ± 0.06	1.8	94	66
Static $SUV_{mean,total}$	0.87 ± 0.06	2.2	100	66
Static $SUV_{mean,median}$	0.86 ± 0.06	2.3	100	66
Static $SUV_{max,total}$	0.85 ± 0.07	2.8	89	73
Static $SUV_{max,late}$	0.81 ± 0.07	2.0	100	53
Static $SUV_{max,median}$	0.80 ± 0.08	3.8	78	80
Newly diagnosed tumors				
Dynamic k_1	0.88 ± 0.08	0.193	60	100
Static $SUV_{max,total}$	0.87 ± 0.08	2.8	90	80
Static $SUV_{mean,late}$	0.85 ± 0.09	2.5	70	90
Static $SUV_{mean,total}$	0.84 ± 0.09	2.4	90	80
Static $SUV_{mean,median}$	0.82 ± 0.10	2.8	80	80
Static $SUV_{max,late}$	0.78 ± 0.11	2.9	80	80
Static $SUV_{max,median}$	0.78 ± 0.11	3.8	80	80
Recurrent tumors				
Dynamic k_1	0.97 ± 0.04	0.194	88	100
Static $SUV_{mean,late}$	0.95 ± 0.06	1.8	100	80
Static $SUV_{mean,total}$	0.95 ± 0.06	2.2	100	80
Static $SUV_{mean,median}$	0.95 ± 0.06	2.4	100	80
Static $SUV_{max,total}$	0.80 ± 0.13	3.2	88	80
Static $SUV_{max,late}$	0.78 ± 0.13	2.0	100	60
Static $SUV_{max,median}$	0.78 ± 0.13	3.0	88	80

after injection and at 60 minutes after injection might still be worth investigating.

Our results are also consistent with the results of Fueger et al,[9] who found SUV_{max} of HG tumor to be 4.2 (1.3) versus SUV_{max} of LG tumor to be 2.3 (1.3) ($P = 0.005$) for newly diagnosed tumors (20-minute acquisition starting at 10 minutes after injection), whereas we observed SUV_{max} of HG tumor to be 4.0 (1.3) versus SUV_{max} of LG tumor to be 2.5 (1.0) ($P = 0.008$, 40-minute acquisition starting at 3 minutes after injection).

If only static imaging is available, our recommendation is thus to measure SUV_{mean}, preferably at late times. It yields high AUC whatever the tumor type (newly diagnosed or recurrent tumors) (Table 4). The LG and HG tumors could be distinguished using $SUV_{mean,late}$ of a 5-minute static ^{18}F-FDopa PET acquisition starting at 38 minutes after injection, which is easily feasible in clinical routine.

Dynamic Imaging for Grading Tumors

For kinetic analysis, we estimated the AIF in the aorta instead of the middle cerebral artery to minimize partial volume effect. Other brain studies have used AIF measured in the aorta for measurements of cerebral glucose metabolism with FDG.[10] When considering AIF in the transverse sinus, Schiepers et al obtained $k_1 = 0.347$ (0.399) (newly diagnosed tumors), that is, a coefficient of variation of 1.15. In our results, we had $k_1 = 0.244$ (0.098) (coefficient of variation of 0.40) suggesting a smaller variability of our approach, possibly due to less uncertainty introduced by partial volume correction. The mean differences between the absolute k_1 and k_2 values reported in Schiepers et al[8] and ours (in newly diagnosed tumors) were $\delta k_1 = 0.103$ and $\delta k_2 = 0.106$ for HG. These differences are partly explained by the different approaches to estimate the AIF. An important conclusion is that the discriminating power of k_1 was demonstrated in both studies, suggesting that the discrimination is robust with respect to potential bias in AIF estimates.

We repeated all analyses using a 3-compartment model.[6] The results (not shown) were very close to those described in this article with the 2-compartment model, and the transport rate k_3 was always close to zero. The differences obtained when considering the 2- or 3-compartment model were $\delta k_1 = 0.0042$ (0.0060) (NS) and $\delta k_2 = 0.0014$ (0.0015) (NS). All conclusions of this study were exactly the same for the 2 models.

The k_1 parameter could clearly distinguish between LG and HG tumors for newly diagnosed lesions ($P = 0.005$), recurrent lesions ($P < 0.02$), and all lesions ($P = 0.001$) unlike k_2 parameter. When considering all tumors, the AUC for k_1 (0.92 [0.05]) was higher than that for $SUV_{mean,late}$ (0.88 [0.06]) although the difference was not significant.

For all tumor groups, the AUC measured when discriminating between HG and LG tumors was always higher with k_1 compared with any SUV. Yet, the difference was never significant, suggesting that the increased complexity associated with dynamic imaging compared with static imaging does not bring significantly increased accuracy in differential diagnosis.

Unlike Chen et al[7] who found no difference in TAC shapes between HG and LG tumors, our HG tumor curves were always characterized by a faster rise of uptake than the LG tumor curves (Fig. 2).

The highest tracer uptake in the tumor generally occurred between 5 minutes and 12 minutes after injection in our study, with mean (SD) time of 8.5 (1.6) minutes for HG tumors and 8.0 (2.9) minutes for LG tumors. This is slightly earlier than reported by Schiepers et al[8] (12.7 minutes for HG tumors, 15.7 minutes for LG tumors) and by Chen et al[7] (between 10 and 30 minutes). The differences in peak times in these studies might be explained by different injection protocols (no description of the injection protocols in Schiepers et al[8] and Chen et al[7]).

In their publication, Schiepers et al[8] used the 2-compartment model, with similar imaging and processing procedures as ours. They found $k_1 = 0.285$ per minute and $k_2 = 0.195$ per minute for 18 HG tumors and $k_1 = 0.170$ per minute and $k_2 = 0.145$ per minute for 11 LG tumors. They reported a statistically significant difference between LG and HG tumors for k_1 ($P < 0.01$), similar to our findings where k_1 discriminated between LG and HG tumors with $P < 0.002$ for all tumor groups. Compared with Schiepers et al, we demonstrated that HG-LG differential diagnosis could also be obtained using static imaging only, without the need for an AIF estimate.

Finally, the higher transport k_1 found in HG tumors compared with LG tumors was observed regardless of whether the tumor was newly diagnosed or recurrent.

CONCLUSIONS

Our work confirmed the usefulness of ^{18}F-FDopa for differential diagnosis between LG and HG glioma in newly diagnosed tumors. We demonstrated for the first time that LG and HG tumors could be distinguished in recurrent gliomas using static ^{18}F-FDopa PET. LG and HG tumors could be distinguished using $SUV_{mean,late}$ of a 5-minute static ^{18}F-FDopa PET acquisition performed 38 minutes after injection. The discrimination was slightly but not significantly improved when dynamic images were acquired and analyzed using a 2-compartment model and an image-derived arterial input function. These results suggest that accurate glioma grading is achievable using static ^{18}F-FDopa PET/CT without the need to perform any blood sampling.

ACKNOWLEDGMENTS

The authors are grateful to Dr. Cyrus Chargari for his helpful suggestions.

REFERENCES

1. Price S. Advances in imaging low-grade gliomas. *Adv Tech Stand Neurosurg*. 2010;35:1–34.
2. Heiss W, Wienhard K, Wagner R, et al. F-Dopa as an amino acid tracer to detect brain tumours. *J Nucl Med*. 1996;37:1180–1182.
3. Herholz K, Hölzer T, Bauer B, et al. ^{11}C-methionine PET for differential diagnosis of low-grade gliomas. *Neurology.* 1998;50:1316–1322.
4. Becherer A, Karanikas G, Szabo M, et al. Brain tumour imaging with PET: a comparison between [18F]fluorodopa and [11C]methionine. *Eur J Nucl Med Mol Imaging*. 2003;30:1561–1567.
5. Tripathi M, Sharma R, D'Souza M. Comparative evaluation of F-18 FDOPA, F-18 FDG, and F-18 FLT-PET/CT for metabolic imaging of low grade gliomas. *Clin Nucl Med*. 2009;34:878–883.
6. Dimitrakopoulou-Strauss A, Strauss L. Quantitative studies using positron emission tomography (PET) for the diagnosis and therapy planning of oncological patients. *Hell J Nucl Med*. 2006;9:10–21.
7. Chen W, Silverman D, Delaloye S, et al. ^{18}F-FDOPA PET imaging of brain tumours: comparison study with ^{18}F-FDG PET and evaluation of diagnostic accuracy. *J Nucl Med*. 2006;47:904–911.
8. Schiepers C, Chen W, Cloughesy T, et al. ^{18}F-FDOPA kinetics in brain tumours. *J Nucl Med*. 2007;48:1651–1661.
9. Fueger BJ, Czernin J, Cloughesy T, et al. Correlation of 6-^{18}F-fluoro-L-Dopa PET uptake with proliferation and tumour grade in newly diagnosed and recurrent gliomas. *J Nucl Med*. 2010;51:1532–1538.
10. Dhawan V, Takikawa S, Robeson W, et al. Quantitative brain FDG/PET studies using dynamic aortic imaging. *Phys Med Biol*. 1994;39:1475–1487.
11. Soret M, Bacharach SL, Buvat I. Partial-volume effect in PET tumour imaging. *J Nucl Med*. 2007;48:932–945.
12. Sing T, Sander O, Beerenwinkel N, et al. ROCR: visualizing classifier performance in R. *Bioinformatics*. 2005;21:3940–3941.
13. Lawson C, Hanson R. *Solving Least Squares Problems*. Englewood Cliffs, NJ; Prentice-Hall; 1974.
14. Hanley JA, McNeil BJ. The meaning and use of the area under a receiver operating characteristic (ROC) curve. *Radiology.* 1982;143:29–36.